

Oscillating pulsar polar gaps

Qinghuan Luo and Don Melrose

School of Physics, The University of Sydney, NSW 2006, Australia

— Received in original form September, 2007

ABSTRACT

An analytical model for oscillating pair creation above the pulsar polar cap is presented in which the parallel electric field is treated as a large amplitude, superluminal, electrostatic wave. An exact formalism for such wave is derived in one-dimension and applied to both the low-density regime in which the pair plasma density is much lower than the corotating charge density and the high-density regime in which the pair plasma density is much higher than the corotating charge density. In the low-density regime, which is relevant during the phase leading to a pair cascade, a parallel electric field develops resulting in rapid acceleration of particles. The rapid acceleration leads to bursts of pair production and the system switches to the oscillatory phase, corresponding to the high density regime, in which pairs oscillate with net drift motion in the direction of wave propagation. Oscillating pairs lead to a current that oscillates with large amplitude about the Goldreich-Julian current. The drift motion can be highly relativistic if the phase speed of large amplitude waves is moderately higher than the speed of light. Thus, the model predicts a relativistic outflow of pairs, a feature that is required for avoiding overheating of the pulsar polar cap and is also needed for the pulsar wind.

Key words: pulsar – particle acceleration – radiation mechanism: nonthermal

1 INTRODUCTION

One of the central problems in pulsar electrodynamics is the production of the relativistic electron-positron pair plasma in which coherent radio emission is thought to be produced (Sturrock 1971). It is widely believed that particles are accelerated to ultra high energy along open field lines, leading to a cascade producing the pair plasma. The pair cascades should produce detectable X-rays and gamma-rays in the case of fast rotating, young pulsars and millisecond pulsars (Thompson 2001). Different acceleration locations in the pulsar magnetosphere have been postulated, with a common feature that the acceleration results from a large scale electric field on open field lines that extend beyond the light cylinder. Acceleration regions in a pulsar magnetosphere are referred to as ‘gaps’. A widely-discussed acceleration region is near the polar cap, for which there is a class of acceleration models called polar gap models (Sturrock 1971; Arons & Scharlemann 1979; Harding & Muslimov 1998). Particle acceleration near the polar cap is of particular relevance for pulsar radio emission since the radio observations suggest that for many pulsars the emission originates deep inside the pulsar magnetospheres (Blaskiewicz, Cordes & Wasserman 1991; Everett & Weisberg 2001). Other acceleration sites include regions in the outer magnetosphere near the null surface,

referred to as outer gaps (Cheng, Ho & Ruderman 1986; Romani 1996; Hirotani 2006) and a variant, referred to as slot gaps, characterized by a long, thin region along the last open field lines (Arons 1983; Harding & Muslimov 2005). Here we concentrate on the polar cap region.

The conventional polar gap models were developed on the basis that the system can settle into a steady state, such that all physical quantities in the pulsar’s corotating frame can be regarded as time-independent (Arons & Scharlemann 1979; Harding & Muslimov 1998). This time-independent assumption is not realistic in practice because it ignores inductive electric fields. There is a strong argument that a time-dependent inductive field plays a central role in pulsar electrodynamics. A global current must be present in the system to form a current closure (Scharlemann & Wagoner 1973; Michel 1975; Cheng & Ruderman 1976; Shibata 1991) and the steady-state assumption requires that the current density, \mathbf{J} , balance $\nabla \times \mathbf{B}/\mu_0$. Moreover, the global electrodynamics requires that the current be determined globally, rather than by local processes near the polar cap (Shibata 1991; Timokhin 2006). The global and local requirements on the current density are generally incompatible without an additional source of charge and current, and any resulting mismatch between \mathbf{J} and $\nabla \times \mathbf{B}/\mu_0$ implies a time-dependent electric field. Such a mismatch and associated inductive electric field seem unavoidable.

Although the idea that a cascade above the polar cap is intrinsically time-dependent was suggested much earlier by Sturrock (1971) and adopted in Ruderman & Sutherland (1975)'s spark model, there are no quantitative models that take into account the time dependence. Levinson et al. (2005) recently discussed an oscillatory gap model to illustrate the time dependent nature of the polar gap in the one-dimensional approximation. In this model, induction currents due to temporal changes in the system are included and particle acceleration is shown to settle into an oscillatory state, similar to a large amplitude wave. The model has several limitations. First, escape of particles is included only implicitly, and escape needs to be made explicit to be consistent with observations of pulsar winds. Second, the oscillatory model is based on numerical integration of the relevant fluid equations together with Maxwell's equations in one dimension and due to the limit of numerical calculation the oscillations could be followed only for a limited number of periods. Third, the assumption that the oscillations are purely temporal is unrealistic, and needs to be generalized to allow outward propagating waves.

In this paper we adopt a different approach, treating the oscillations as a large-amplitude electrostatic wave (LAEW) in a cold pair plasma. Although LAEW in a cold electron gas was discussed in Akhiezer et al. (1975), to our knowledge there has been no discussion of the case of a strongly magnetized, electron-positron pair plasma. Relativistic motion of a single particle in a LAEW was discussed and applied to pulsar emission by Rowe (1992a,b). However, in the single-particle treatment, the wave was assumed to pre-exist and feedback of the particle's motion on the wave field was not taken into account. Here we treat the electrons and positrons as cold fluids and determine particle acceleration by solving simultaneously both fluid equations and Maxwell's equations without making an a priori assumption of time-independence. We include pair creation in our equations, but neglect it in deriving analytic solutions.

In Sec 2 we outline the fluid formalism for time-dependent electrodynamics that includes inductive electric fields. Analytical solutions for LAEW are described in Sec 3. Inclusion of pair production in LAEW is discussed Sec 4 and the low-density limit is discussed in Sec 5.

2 TIME-DEPENDENT FORMALISM

2.1 Fluid equations

We consider a two-component cold fluid consisting of electrons and positrons; the fluid number density and velocity are denoted by N_{\pm} and \mathbf{v}_{\pm} , where the subscripts \pm correspond respectively to the positron and electron components. In the observer's inertial frame, a pulsar rotates with an angular velocity $\Omega = 2\pi/P$, where P is the pulsar period. Provided that sufficient charge density is available, the corotating electric field is set up so that charged particles corotate with the star. This electric field can be eliminated by choosing a frame corotating with the star. Well inside the light cylinder, the corotating frame and observer's inertial frame are connected by a local Galilean transformation with velocity $\mathbf{v}_R = \Omega \times \mathbf{r}$, where \mathbf{r} is the radial vector directed from the star's center to a point of interest. One has $|v_R/c| \sim r/R_{LC}$,

with $R_{LC} = c/\Omega$ the light-cylinder radius. Thus, the effect on the rotation of the fluids can be neglected if the region concerned is close to the polar cap where $r/R_{LC} \ll 1$.

The relevant fluid equations, the continuity equation and equation of motion, can be written down as

$$\frac{\partial N_{\pm}}{\partial t} + \nabla \cdot (N_{\pm} \mathbf{v}_{\pm}) = \frac{1}{2} Q, \quad (1)$$

$$\left(\frac{\partial}{\partial t} + \mathbf{v}_{\pm} \cdot \nabla \right) \mathbf{u}_{\pm} = \pm \frac{e\mathbf{E}}{m_e c} + \frac{\mathbf{q}_{\pm}}{m_e c^2} - \frac{Q}{2N_{\pm}} \mathbf{u}_{\pm}, \quad (2)$$

where \mathbf{q}_{\pm} is radiation drag, Q is a source function due to pair production and $\mathbf{u}_{\pm} = \gamma_{\pm} \mathbf{v}_{\pm}/c$ is the particle's dimensionless momentum. The Lorentz force is absent because all the particles are assumed to be in the ground Landau state. The current and charge densities are

$$\mathbf{J} = e \sum_{s=\pm} s \mathbf{v}_s N_s, \quad \rho = e \sum_{s=\pm} s N_s, \quad (3)$$

with $s = \pm$. The fluid equations are supplemented by Maxwell's equations, written in the corotating frame. The two relevant Maxwell equations involve the charge density and current density (Fawley, Arons & Scharlemann 1977)

$$\nabla \cdot \mathbf{E} = \frac{1}{\varepsilon_0} (\rho - \rho_{GJ}), \quad (4)$$

$$\nabla \times \mathbf{B} = \mu_0 (\mathbf{J} - \mathbf{J}_R) + \frac{1}{c^2} \frac{\partial \mathbf{E}}{\partial t}, \quad (5)$$

where $\rho_{GJ} = \varepsilon_0 [-2\Omega \cdot \mathbf{B} + (\Omega \times \mathbf{r}) \cdot (\nabla \times \mathbf{B})]$ is the Goldreich-Julian (GJ) density. Here we ignore the general relativistic effects such as frame dragging (cf. Sec 5.2). In (5) \mathbf{J}_R is a vectorial sum of all the remaining terms that are small for $r/R_{LC} \ll 1$; the full expression for \mathbf{J}_R is given by (A5) in Fawley, Arons & Scharlemann (1977) and it is neglected here. Equation (4) describes a noncorotating electric field arising from deviation of charge density from the GJ density. In steady-state models, equation (5) is (implicitly) assumed to be satisfied trivially. However, it plays a central role here in determining the inductive field arising from a current mismatch.

The inclusion of the inductive field distinguishes the model considered here from steady-state polar-gap models in which only Poisson's equation (i.e., Eq 4) is relevant and the parallel electric field is treated as static (Arons & Scharlemann 1979; Harding & Muslimov 1998). The static assumption is incompatible, in general, with the constraint imposed by a global current. It has long been recognized that circulation of a global current plays a critical role in dissipation of rotational energy of pulsars (Scharlemann & Wagoner 1973; Michel 1975; Cheng & Ruderman 1976). Such current, denoted by \mathbf{J}_0 , should be determined globally. The simplest case is where the global current is assumed to be a constant. Assuming $\mathbf{J}_{0\parallel} = (\nabla \times \mathbf{B})_{\parallel}$, where \parallel represents projection along the magnetic field, the steady-state assumption implies that the local current exactly matches the global current, $\mathbf{J}_{\parallel} = \mathbf{J}_{0\parallel}$ (when \mathbf{J}_R is ignored), everywhere. This assumption is not realistic, for example, due to pair creation changing the current density locally (Levinson et al. 2005). In our oscillatory model, the parallel electric field is treated predominantly as an inductive field due to oscillation of the current about the global constant direct current. Relevant solutions are oscillatory and should be treated as large amplitude waves.

2.2 Large amplitude waves

We outline a general approach for deriving a time-dependent solution in which oscillations are considered as a large amplitude wave propagating in the direction $\boldsymbol{\kappa}$ at a constant phase speed β_V (in units of c). We assume that oscillatory quantities are functions of

$$\chi = \omega_{GJ} \left(\beta_V t - \frac{\boldsymbol{\kappa} \cdot \mathbf{r}}{c} \right), \quad (6)$$

where $\omega_{GJ} = (e^2 N_{GJ} / \varepsilon_0 m_e)^{1/2}$ is the plasma frequency at the GJ number density, $N_{GJ} = 2\varepsilon_0 \Omega B_0 / e$, and B_0 is the surface magnetic field. We normalize the electric field as $\tilde{E}_{\parallel} = eE_{\parallel} / m_e c \omega_{GJ}$, density as $\tilde{N}_{\pm} = N_{\pm} / N_{GJ}$, the charge density as $\eta = \rho / e c N_{GJ}$ and the current density as $\mathbf{j} = \mathbf{J} / e c N_{GJ}$. Using $\partial/\partial t = \omega_{GJ} \beta_V d/d\chi$ and $\boldsymbol{\nabla} \equiv \partial/\partial \mathbf{r} = -(\omega_{GJ} \boldsymbol{\kappa} / c) d/d\chi$, one may write (1), (2) and (5) in the dimensionless forms

$$\frac{d}{d\chi} \left[(\beta_V - \boldsymbol{\kappa} \cdot \boldsymbol{\beta}_{\pm}) \tilde{N}_{\pm} \right] = \frac{1}{2} \tilde{Q}, \quad (7)$$

$$(\beta_V - \boldsymbol{\kappa} \cdot \boldsymbol{\beta}_{\pm}) \frac{d\mathbf{u}_{\pm}}{d\chi} = \pm \tilde{\mathbf{E}} + \tilde{\mathbf{q}}_{\pm} - \frac{\tilde{Q}}{2\tilde{N}_{\pm}} \mathbf{u}_{\pm}, \quad (8)$$

$$\left[(1 - \beta_V^2) \mathbf{I} - \boldsymbol{\kappa} \boldsymbol{\kappa} \right] \cdot \frac{d\tilde{\mathbf{E}}}{d\chi} = \beta_V (\mathbf{j} - \mathbf{j}_0), \quad (9)$$

where $\boldsymbol{\beta}_{\pm} = \mathbf{v}_{\pm} / c$, $\tilde{\mathbf{q}}_{\pm} = \mathbf{q}_{\pm} / (m_e c^2 \omega_{GJ})$, $\tilde{Q} = Q / (N_{GJ} \omega_{GJ})$, $(\mathbf{I})_{ij} = \delta_{ij}$ and $\mathbf{j}_0 = \boldsymbol{\nabla} \times \mathbf{B} / (e N_{GJ} c)$ which is assumed to be a constant vector. Poisson's equation (4) and the induction equation (5) may be replaced by the equation of charge continuity and the induction equation. With the charge and current densities functions only of χ , the equation of charge continuity gives

$$\frac{d}{d\chi} (\beta_V \eta - \boldsymbol{\kappa} \cdot \mathbf{j}) = 0. \quad (10)$$

Note that in our model both Poisson's equation and the induction equation contribute. The steady state models correspond to the limit $\beta_V \rightarrow 0$, and hence $\boldsymbol{\kappa} \cdot \mathbf{j} = \text{const.}$, when the induction equation does not contribute. It is only in the opposite limit, $\beta_V \rightarrow \infty$, where the oscillations are purely temporal, that Poisson's equation makes no contribution (cf. Sec 2.3). As we are primarily interested in oscillatory solutions, in deriving these equations we ignore inhomogeneity, notably in the magnetic field. This neglect is justified provided that the spatial scale for the inhomogeneity is much larger than the oscillation length. The scale of the inhomogeneity is of order the radius of curvature, which at a height $r - R$ with $R = 10^4$ m the star's radius, is larger than but of order $(r R_{LC})^{1/2}$. One has $\sim (r R_{LC})^{1/2} \approx 2.2 \times 10^5 (r/R)^{1/2} P_{0.1}^{1/2}$ m, where $P_{0.1} = P/0.1$ s. For plausible parameters, this is much larger than the oscillation length, which is of order

$$\begin{aligned} \lambda &= \frac{c\beta_V}{\omega_{GJ}} \left(\frac{\gamma}{\tilde{N}} \right)^{1/2} \\ &\approx 0.9\beta_V B_8^{1/2} P_{0.1}^{-1/2} \left(\frac{\gamma}{10^6} \right)^{1/2} \left(\frac{\tilde{N}}{10^2} \right)^{-1/2} \text{ m}, \end{aligned} \quad (11)$$

with $B_8 = B_0 / 10^8$ T, $\tilde{N} = \max\{\tilde{N}_+, \tilde{N}_-\}$ and where we assume an oscillation frequency $\sim \omega_p / \gamma^{1/2}$ (see Eq 33). For the numerical example in (11), the condition is satisfied provided that $\beta_V < 2.4 \times 10^5$. We are only concerned with the open

field line region which can be regarded as a flux tube with a conducting surface, defined by the last closed field lines, that separates the region from the closed field line region. Eq (7)–(9) are then valid only when the wavelength is much shorter than the transverse size $\sim (r/R_{LC})^{1/2} r \geq 258 P_{0.1}^{-1/2}$ m. Such short wavelength approximation implies that the limit $\beta_V \rightarrow \infty$ is not applicable for pulsars. Nonetheless, such limit is also discussed here as it simplifies the formalism from which the basic properties of LAEWs can be derived and compared to a more general case where β_V is finite.

Integration of Eq (7) yields an exact form for the density

$$\tilde{N}_{\pm} = \frac{(\beta_V - \boldsymbol{\kappa} \cdot \boldsymbol{\beta}_{\pm}) n_{\pm} + F_Q}{\beta_V - \boldsymbol{\kappa} \cdot \boldsymbol{\beta}_{\pm}}, \quad F_Q = \frac{1}{2} \int_0^{\chi} \tilde{Q}(\chi') d\chi', \quad (12)$$

where $n_{\pm} = \tilde{N}_{\pm}(0)$ is the initial density at $\chi = 0$, $\boldsymbol{\beta}_{\pm 0}$ are the initial velocities (in units of c), and F_Q is a cumulative flux arising from pair creation. A wave is classified as superluminal if $\beta_V > 1$, luminal if $\beta_V = 1$ and subluminal if $\beta_V < 1$. We do not consider the subluminal case here. For superluminal and luminal waves, \tilde{N}_{\pm} is always positive. The number density remains approximately constant in a superluminal wave in the limit $\beta_V \rightarrow \infty$.

2.3 Current-charge invariant

The charge continuity equation (10) implies an invariant $\boldsymbol{\kappa} \cdot \mathbf{j} - \beta_V \eta = \text{const.}$ Denoting the dimensionless current density by $j_{\parallel} = \boldsymbol{\kappa} \cdot \mathbf{j}$, this conservation law implies

$$j_{\parallel}(\chi) - \beta_V \eta(\chi) = j_{\parallel}(0) - \beta_V \eta(0), \quad (13)$$

where $\chi = 0$ corresponds to the initial conditions, with $j_{\parallel}(0) = \beta_{+0} n_+ - \beta_{-0} n_-$, $\eta(0) = n_+ - n_-$. The steady state condition corresponds to the special limit $\beta_V \rightarrow 0$, and in this limit the induction equation is satisfied trivially with $j_{\parallel} = j_{0\parallel}$. The constant current \mathbf{j}_0 is interpreted as the global direct current, assumed to be determined by global conditions and to be a free parameter in the theory. In steady state models, only Poisson's equation is relevant and the constant current $j_{0\parallel}$ does not appear explicitly. For $\beta_V \neq 0$, it is convenient to write $\eta_{GJ} = \rho_{GJ} / e N_{GJ}$, for the sign of the GJ charge density, and to write the right hand side of Eq (13) in the form

$$j_{\parallel}(0) - \beta_V \eta(0) = j_{0\parallel} - \beta_V \eta_{GJ}. \quad (14)$$

The opposite limit $\beta_V \rightarrow \infty$ corresponds to purely temporal oscillations. In this case (14) requires that the charge density equal the GJ density, so that Poisson's equation is satisfied trivially. We are interested in the general case $0 < \beta_V < \infty$.

Assuming a strong magnetic field approximation, a plausible simplifying assumption is that $\boldsymbol{\kappa}$ is directed along the magnetic field. The problem then becomes one dimensional, involving only projections of the relevant equations along the magnetic field. Of particular significance is $j_{0\parallel}$, which would be identically zero if the magnetic field were dipolar. The global requirement for $j_{0\parallel} \neq 0$ implies a nonzero azimuthal magnetic field $B_{\phi} \sim (r/R_{LC}) j_{0\parallel} B \ll B$ (see further discussion in Sec 3.4). Although $j_{0\parallel}$ cannot be determined locally, it is plausible to assume that it has the same sign as η_{GJ} , i.e., $j_{0\parallel} < 0$ for $\boldsymbol{\Omega} \cdot \mathbf{B} > 0$ and $j_{0\parallel} > 0$ for $\boldsymbol{\Omega} \cdot \mathbf{B} < 0$.

One may use (13) and (14) to express β_V in terms of the initial density and velocity:

$$\beta_V = \frac{j_{0\parallel} - \beta_{+0}n_+ + \beta_{-0}n_-}{\eta_{GJ} - n_+ + n_-}, \quad (15)$$

provided that $\eta(0) = n_+ - n_- \neq \eta_{GJ}$. The following three cases are of interest: the initial charge density matches the GJ density $\delta\eta = \eta_{GJ} - \eta(0) = 0$, the initial charge density has a small deviation from the GJ density $|\delta\eta| \ll 1$, and pair density is much lower than the GJ density $n_{\pm} \ll 1$. In the first case, one must have $j_{\parallel}(0) = j_{0\parallel}$ and thus, the phase speed is not constrained by (14). Generally, the second applies to polar cap regions where both frame-dragging and field line curvature may cause a small deviation of a charge density from the corotation density (Arons & Scharlemann 1979; Shibata 1997; Harding & Muslimov 1998). Eq (15) implies $|\beta_V| \gg 1$ for $|\delta\eta| \ll |1 - \beta_0|$, $j_{0\parallel} = \eta_{GJ}$ and $\beta_0 = \beta_{+0} \approx \beta_{-0}$. Therefore, the LAEW considered here should be superluminal. In the third case, one has $\beta_V \approx j_{0\parallel}/\eta_{GJ}$; the wave is superluminal for $j_{0\parallel} > \eta_{GJ}$ and subluminal for $j_{0\parallel} < \eta_{GJ}$.

3 LARGE AMPLITUDE, ELECTROSTATIC WAVES

We consider large amplitude, electrostatic waves in a high density regime where the density of pairs is much higher than the GJ density, $n_{\pm} \gg 1$, and pair creation is absent. This regime is especially applicable when the system undergoes a brief burst of pair production leading to a pair plasma with $n_{\pm} \gg 1$ and sets up oscillations.

To concentrate on the basic physics of such large amplitude waves we ignore the radiation drag, $\tilde{q}_{\pm} = 0$. Eqs (9) and (8) reduce to the following simple forms:

$$\frac{d\tilde{E}_{\parallel}}{d\chi} = \frac{j_{0\parallel}}{\beta_V} - \frac{1}{\beta_V} \sum_{s=\pm} s\beta_s \frac{(\beta_V - \beta_{s0})n_s}{\beta_V - \beta_s}. \quad (16)$$

$$\frac{d}{d\chi} \frac{1 - \beta_V\beta_{\pm}}{(1 - \beta_{\pm}^2)^{1/2}} = \mp \tilde{E}_{\parallel}. \quad (17)$$

Integration of (17) leads to the following invariant:

$$\sum_{s=\pm} \frac{1 - \beta_V\beta_s}{(1 - \beta_s^2)^{1/2}} = \sum_{s=\pm} \frac{1 - \beta_V\beta_{s0}}{(1 - \beta_{s0}^2)^{1/2}} \equiv \xi_1. \quad (18)$$

One needs to consider only one component of the fluid, say the electron (−) and the solution for the other component can be derived using (18). Plots of β_+ as a function of β_- are shown in figure 1 for luminal and superluminal waves. Using the notation

$$\xi \equiv \frac{1 - \beta_V\beta_-}{(1 - \beta_-^2)^{1/2}}, \quad (19)$$

the velocity can be expressed in terms of ξ :

$$\beta_-(\xi) = \frac{\beta_V - \xi(\beta_V^2 + \xi^2 - 1)^{1/2}}{\beta_V^2 + \xi^2}, \quad (20)$$

$$\beta_+(\xi) = \beta_-(\xi_1 - \xi). \quad (21)$$

Notice that the two velocities (20) and (21) are related by a transform $\xi \rightarrow \xi_1 - \xi$. Exact solutions to (16) and (17) are

$$-\int \frac{d\xi}{\Phi^{1/2}(\xi)} = \chi, \quad (22)$$

$$\tilde{E}_{\parallel} = \pm \Phi^{1/2}, \quad (23)$$

with

$$\Phi(\xi) = \tilde{E}_0^2 + \frac{2}{\beta_V} \left[(\xi - \xi_0)j_0 - (\beta_V - \beta_{+0})g(\xi)n_+ - (\beta_V - \beta_{-0})(\gamma_-(\xi) - \gamma_{-0})n_- \right], \quad (24)$$

$$g = \int_{\xi_0}^{\xi} \frac{\beta_+(\xi')}{\beta_V - \beta_+(\xi')} d\xi' = -\frac{1}{\beta_V^2 - 1} \left\{ \xi_0 - \xi - \beta_V \left[(\beta_V^2 + (\xi_1 - \xi)^2 - 1)^{1/2} - (\beta_V^2 + (\xi_1 - \xi_0)^2 - 1)^{1/2} \right] \right\}, \quad (25)$$

where $\xi_0 = \xi(0)$ and $\gamma_{-0} = \gamma_-(\xi_0)$ is the initial Lorentz factor of electrons. The initial electric field is $\tilde{E}_0 = \pm \Phi^{1/2}(\xi_1) = d\xi/d\chi$ at $\chi = 0$, where the sign is determined by the sign of $d\xi/d\chi$ at $\chi = 0$. Although we are interested in superluminal waves, the calculation up to this stage applies to any β_V including the special case $\beta_V = 1$. For $\beta_V = 1$, (25) simplifies to $g = [(\xi_1 - \xi)^{-1} - (\xi_1 - \xi_0)^{-1} + \xi_0 - \xi]/2$. The function $g(\xi)$ is shown in figure 3 for superluminal waves $\beta_V > 1$.

3.1 Conditions for an oscillatory solution

The condition for existence of an oscillatory solution for (16) and (17) is $\Phi(\xi) \geq 0$. For $n_{\pm} \gg 1$, (24) simplifies to

$$\Phi \approx \tilde{E}_0^2 - (2/\beta_V)(\beta_V - \beta_{-0})(g + \gamma_- - \gamma_0)n_- \geq 0, \quad (26)$$

where (15) is used to eliminate n_+ . An appropriate approximation to $g(\xi)$ can be derived as follows. In each oscillation a particle's velocity is highly relativistic except for a short phase when it is briefly nonrelativistic and changes sign. In this case, (25) can be approximated by two straight lines that cross at $\xi \approx \xi_1$. For $\beta_{\pm 0} = 0$ (solid and dashed) the minimum is located at $\xi = \xi_1 = 2$. Specifically, for $(\xi_1 - \xi_0)^2 \gg \beta_V^2 - 1$ and $(\xi_1 - \xi)^2 \gg \beta_V^2 - 1$, one has the following approximation

$$g(\xi) \approx \begin{cases} \frac{\xi_0 - \xi_1}{1 + h(\xi_1 - \xi_0)\beta_V} + \frac{\xi - \xi_1}{\beta_V - 1}, & \xi \geq \xi_1, \\ \frac{\xi_0 - \xi_1}{1 + h(\xi_1 - \xi_0)\beta_V} - \frac{\xi - \xi_1}{\beta_V + 1}, & \xi < \xi_1, \end{cases} \quad (27)$$

with $h(x) = 1$ for $x \geq 0$ and $h(x) = -1$ for $x < 0$. In the large β_V limit $g(\xi)$ is symmetric about the vertical axis at $\xi = \xi_1$. As the phase velocity approaches the luminal limit $\beta_V \rightarrow 1$ the right-hand side of the curve steepens and approached the vertical axis. In figure 3, (27) is shown as dotted lines, which gives a quite good approximation to the exact numerical result (solid lines).

The condition (26) leads to upper and lower limits to u_- , given by

$$u_{\max} \approx \frac{1}{2\beta_V} [(\beta_V + 1)\Gamma - \xi_1],$$

$$u_{\min} \approx -\frac{1}{2\beta_V} [(\beta_V - 1)\Gamma + \xi_1], \quad (28)$$

with

$$\Gamma = \gamma_{-0} + \frac{\beta_V \tilde{E}_0^2}{2n_-(\beta_V - \beta_{-0})} - \frac{\xi_0 - \xi_1}{1 + h(\xi_1 - \xi_0)\beta_V}. \quad (29)$$

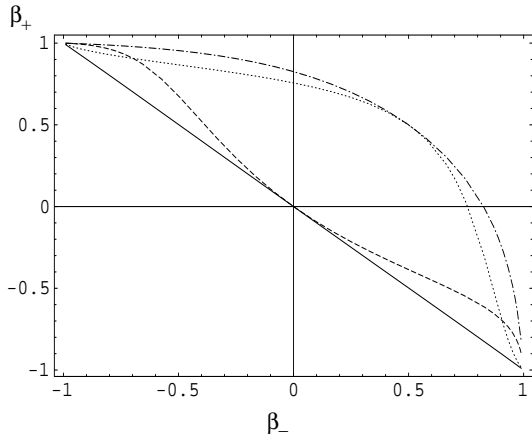
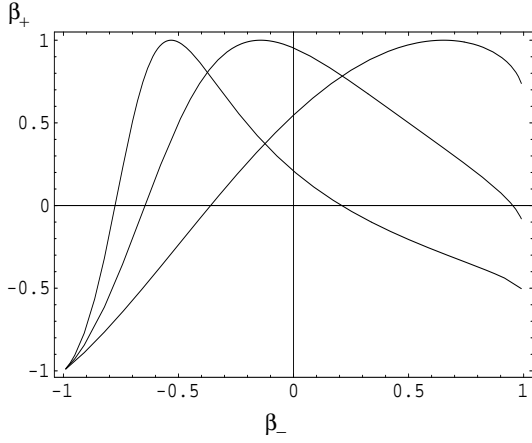


Figure 1. Plot of β_+ as a function of β_- . Upper: $\beta_V = 1$. The curves from left to right correspond to $\beta_{\pm 0} = 0, 0.5$ and 0.9 , respectively. In each case, the physical range corresponds to a range from where a maxima occurs to the rightmost. Lower: $\beta_V = 1.5$ and $\beta_{\pm 0} = 0$ (dashed), $\beta_V = 1.5$ and $\beta_{\pm 0} = 0.5$ (dash-dotted), $\beta_V = 100$ and $\beta_{\pm 0} = 0$ (solid), $\beta_V = 100$ and $\beta_{\pm 0} = 0.5$ (dotted).

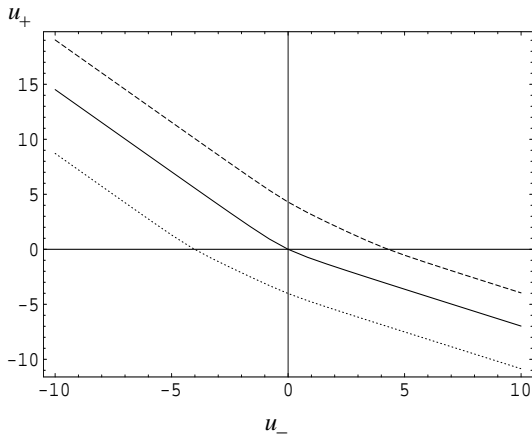


Figure 2. Plot of u_+ as a function of u_- for $\beta_{0\pm} = 0$ (solid), $\beta_{0\pm} = 0.9$ (dashed) and $\beta_{0\pm} = -0.9$ (dotted). Because of $\xi \neq 0$, motions of electrons and positrons are not strictly symmetric about $u_+ \rightarrow -u_-$.

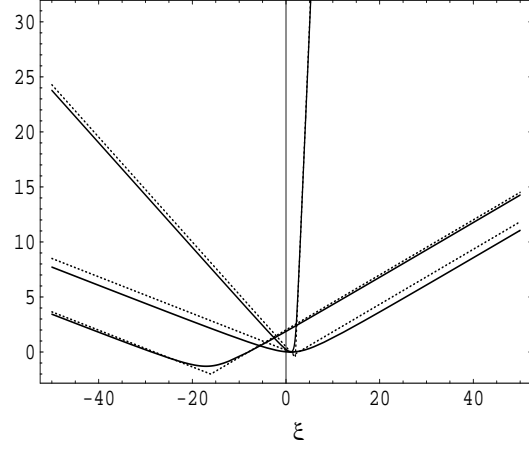


Figure 3. Plot of $g(\xi)$. The three solid V-shaped curves from left to right correspond respectively to $\beta_V = 5$ with $\beta_{\pm 0} = 0.9$, $\beta_V = 5$ with $\beta_{\pm 0} = 0$, and $\beta_V = 1.1$ with $\beta_{\pm 0} = 0$. The minima where the two lines meet are located at $\xi_1 \approx -16$ for the leftmost plot and $\xi = \xi_1 = 2$ for the other two. The dotted lines are obtained using the approximation (27) which consists of two straight lines with gradients $1/(\beta_V - 1)$ and $-1/(\beta_V + 1)$, respectively.

Using (18) the positron momentum u_+ can be expressed in terms of u_- , which leads to the same upper and lower limits for positrons as (28). For luminal waves with $\beta_V = 1$, one has $u_{\max} \approx (1 + \tilde{E}_0^2/n_-)/2$ and $u_{\min} \approx -1$. In this case oscillations skew strongly in the direction of wave propagation. For $\beta_V \rightarrow \infty$, (28) reduces to $u_{\max} = (\Gamma + u_{+0} + u_{-0})/2$ and $u_{\min} = -(\Gamma - u_{+0} - u_{-0})/2$. When $u_{\pm 0} = 0$, oscillations become symmetric with $u_{\max} = -u_{\min} = \Gamma/2$. Since $u_{\max} \neq u_{\min}$, oscillating electrons and positrons have a net drift velocity $\sim (u_{\max} + u_{\min})/2 \approx (\Gamma - \xi_1)/\beta_V$. An accurate evaluation of the drift velocity is given in Sec. 3.3.

Numerical solutions to $E_{\parallel} = 0$ (i.e., $\Phi(\xi) = 0$) are shown as contours in figure 4. We express n_+ in terms of β_V , $j_{0\parallel}$, and η_{GJ} using (13) and (14). In the subfigure on the left one assumes luminal waves with $\beta_V = 1$. Each pair of lines defines an upper limit, u_{\max} , and a lower limit, u_{\min} , to a particle's momentum such that one has $\Phi > 0$ for $u_{\min} < u_- < u_{\max}$. The similar upper and lower limits can be obtained for positrons. Particles oscillate with their momenta confined between these two limits. As $u_{\max} \gg |u_{\min}|$, the oscillations skew strongly in the wave propagation direction. The dotted lines correspond to a superluminal wave $\beta_V = 2$. As β_V increases the system evolves toward symmetric oscillations as shown in the subfigure on the right. A nonzero initial velocity ($\beta_{0\pm} > 0$) also shifts the oscillations forward (dash-dotted lines). It should be emphasized that we intentionally choose a moderate n_- here to illustrate that an oscillatory solution can exist even for a moderate pair density.

3.2 Analytical formalism

To seek an oscillatory solution one may define the oscillation periodicity (in units of $1/\omega_{GJ}$)

$$\hat{T} = \frac{2}{\beta_V} \int_{\chi_a}^{\chi_b} \frac{d\chi}{\Phi^{1/2}} = -\frac{2}{\beta_V} \int_{\xi_a}^{\xi_b} \frac{d\xi}{\Phi^{1/2}(\xi)}, \quad (30)$$

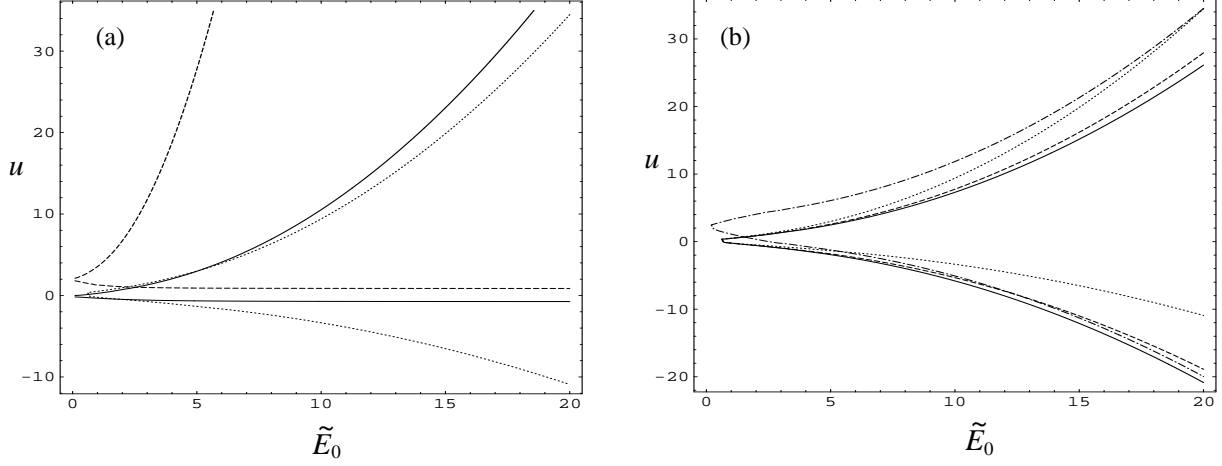


Figure 4. Conditions for $E_{\parallel} = 0$. (a) A luminal wave $\beta_V = 1$, with $n_- = 5$, $j_{0\parallel} = \eta_{GJ} = -1$. The solid and dashed lines correspond to $\beta_{\pm 0} = 0$ and 0.9 , respectively. Each pair of lines defines an upper and lower limits to u , between which $\Phi > 0$. For comparison a superluminal wave with $\beta_V = 2$ and $\beta_{0\pm} = 0$ is shown as a dot line. (b) Superluminal waves with different phase velocities $\beta_V = 2$ (dotted), 10^3 (solid), 10 (dashed). We assume $\beta_{\pm 0} = 0$. The dash-dotted lines represent $\beta_V = 10$ with $\beta_{0\pm} = 0.9$.

where the subscripts a, b label respectively the phases at which $\beta_- = \beta_{\min}$ and $\beta_- = \beta_{\max}$, respectively. The oscillation frequency is then given by $\omega = 2\pi\omega_{GJ}/\hat{T}$, where $\omega_{GJ} \approx (1.5 \times 10^{11} \text{ s}^{-1})P_{0.1}^{-1}B_8$. Using the approximations (27) an analytical solution for a LAEW can be derived. For $\beta_V \gg 1$, using $\gamma_-(\xi) + g(\xi) \sim 2|\xi|/\beta_V$, one obtains the following approximation to (26):

$$\Phi(\xi) \approx 2n_- \left(1 - \frac{\beta_{-0}}{\beta_V}\right) \left(\Gamma \pm \frac{\xi_1 - 2\xi}{\beta_V \mp 1}\right), \quad (31)$$

where the upper and lower signs correspond to $\xi \geq \xi_1$ and $\xi < \xi_1$, respectively. For $\beta_V \gg 1$ one may expand (31) in $1/\beta_V$ and substitute it for (30), obtaining

$$\hat{T} \approx 4 \left[\frac{\beta_V \Gamma}{2n_-(\beta_V - \beta_{-0})} \right]^{1/2} \approx \frac{2\tilde{E}_0}{n_-}. \quad (32)$$

A second approximation applies for $\tilde{E}_0^2/2n_- \gg \gamma_{0\pm}$, in which case one estimates the frequency as

$$\omega \approx \frac{\sqrt{2}\pi\omega_p}{4u_{\max}^{1/2}}, \quad (33)$$

where $\omega_p = (2n_-)^{1/2}\omega_{GJ}$ is the plasma frequency of the pair plasma. As an example, one has $\omega \approx 10^9 \text{ s}^{-1}$ for $n_- = 10^2$, $u_{\max} = 10^6$ and $\omega_{GJ} = 10^{11} \text{ s}^{-1}$. The oscillation frequency decreases as u_{\max} increases, which can be understood as an increase in the effective mass of electrons or positrons.

The condition for $\Phi > 0$ is $|\xi| < \xi_b \approx -\xi_a \approx \beta_V \tilde{E}_0^2/4n_-$; this gives $u_{\max} \approx \tilde{E}_0^2/4n_- \approx -u_{\min}$. Note that such symmetry in oscillation is a direct consequence of our assumption of large β_V and $\beta_{\pm 0} = 0$. The solution for $0 \leq \chi < \chi_T = \beta_V \hat{T}$ is found to be

$$\chi \approx \begin{cases} \frac{\beta_V}{2n_-} (\Phi_0^{1/2} - \Phi^{1/2}), & 0 \leq \chi < \frac{3}{4}\chi_T, \\ \frac{1}{2}\chi_T + \frac{\beta_V}{2n_-} (\Phi_0^{1/2} - \Phi^{1/2}), & \frac{3}{4}\chi_T \leq \chi < \chi_T, \end{cases} \quad (34)$$

where Φ is given by (31), $\Phi_0 = \Phi(1)$, $\Phi_{a,b} = \Phi(\xi_{a,b})$. The electric field is obtained as

$$\tilde{E}_{\parallel} \approx \begin{cases} \tilde{E}_0 + \frac{2n_-}{\beta_V} \chi, & 0 \leq \chi < \chi_T/2, \\ \tilde{E}_0 + \frac{2n_-}{\beta_V} (\chi_T - \chi), & \chi_T/2 \leq \chi < \chi_T. \end{cases} \quad (35)$$

The electric field displays a sawtooth wave form, which can be understood qualitatively in terms of the extreme relativistic limit. In this limit positrons and electrons are accelerated in opposite directions, giving rise to a current $|j_{\parallel}| \sim 2|\beta_-|n_- \gg |j_{0\parallel}| \sim 1$. Thus, the electric field is $E_{\parallel} \propto \pm |j_{\parallel}|/\beta_V \sim \pm 2n_- \chi/\beta_V$ with $|\beta_-| \sim 1$, which reproduces the sawtooth wave form given by (35). An example of a numerical integration of (22) and (23) is shown in figure 5 for pairs with an initial, forward velocity. Figure 6 shows oscillations for particles with an initial velocity toward the star. Although our analytical solution is obtained for $n_- \gg 1$, here we again choose a moderate n_- in the numerical calculation to show that our oscillatory solution is also valid for $n_{\pm} \sim 1$. The wave form is similar to that predicted from the numerical model (Levinson et al. 2005). The characteristics of the oscillations, including the periodicity and amplitude, are independent of the sign of \tilde{E}_0 and are not sensitive to the initial conditions $\beta_{0\pm}$ provided that $|u_{0\pm}| \ll u_{\max}$. As no radiative loss, pair production nor wave damping is included, the wave amplitude remains constant. In the figure we assume an initial electric field much lower than the typical vacuum field $\tilde{E}_{\max} \sim 3 \times 10^6 (B/B_c)^{1/2} P_{0.1}^{-1/2}$, where $B_c \approx 4.4 \times 10^9 \text{ T}$. In practice, the initial field should be near the pair creation threshold. Assuming the pair production threshold to be γ_{th} , one has $\tilde{E}_0 \approx 3 \times 10^4 (n_-/5)^{1/2} (\gamma_{th}/10^6)^{1/2}$ (see discussion in Sec. 5). Since $|u_{\min}| < |u_{\max}|$, the oscillating particles have a net forward flow velocity.

3.3 Drift motion

The drift momentum can be obtained by averaging u_- over one period (\hat{T}):

$$\bar{u} = \frac{2}{\beta_V \hat{T}} \int_{\chi_a}^{\chi_b} u_- d\chi \approx \frac{2\Gamma}{3\beta_V} \left(1 - \frac{3\xi_1}{4\Gamma}\right), \quad (36)$$

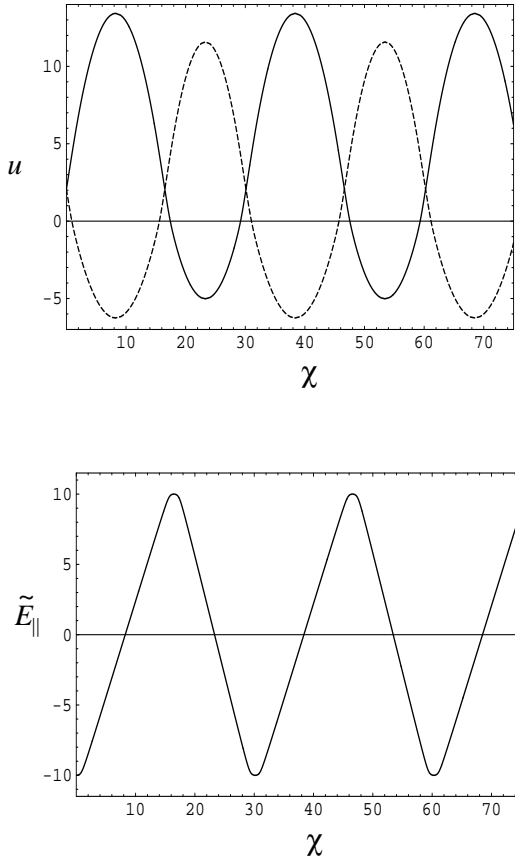


Figure 5. Dimensionless momentum u (upper) and electric field \tilde{E}_{\parallel} (lower) as functions of phase χ . The dashed line corresponds to oscillations of positrons. As there is no dissipation included, the amplitudes of the oscillations are determined by $|\tilde{E}_0|$. Electrons oscillate between $u_{\min} \approx -5.0$ and $u_{\max} \approx 13.4$, with a net drift velocity $\bar{u} \approx 3.6$. Oscillations of positrons (dashed) skew less in the positive direction than electrons. We assume $\tilde{E}_0 = -10$, $\beta_V = 5$, $\beta_{\pm 0} = 0.9$, $j_{0\parallel} = \eta_{GJ} = -1$, $n_- = 5$.

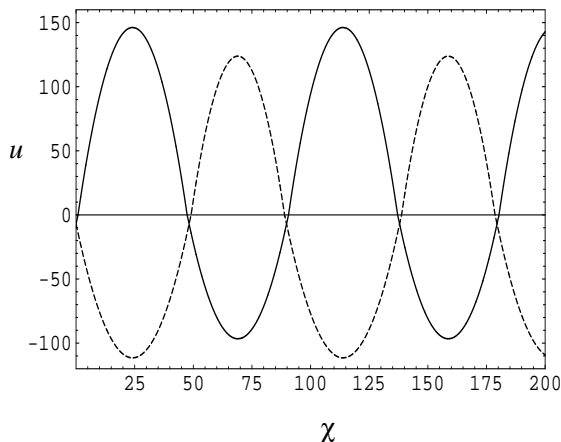


Figure 6. As in figure 5 but with $\beta_{\pm 0} = -0.99$, $\tilde{E}_0 = -50$. The oscillation pattern is similar to figure 5 but with a small backward shift.

where we expand Φ on $1/\beta_V \ll 1$ and change the integration variable to $d\chi = -d\xi/\Phi^{1/2}(\xi)$. Terms of order $|j_{0\parallel}|/n_{\pm} \ll 1$ and $|\eta_{GJ}|/n_{\pm} \ll 1$ are ignored. Then both electrons and positrons are dragged along in the wave at the same drift velocity $\beta_D = \bar{u}/(1 + \bar{u}^2)^{1/2}$. For $\tilde{E}_0^2/2n_- \gg \gamma_{\pm 0}$ one has

$$\bar{u} \approx \frac{\tilde{E}_0^2}{3n_- \beta_V} \approx \frac{4u_{\max}}{3\beta_V}. \quad (37)$$

The drift velocity decreases as the wave phase speed increases. In the limit $\beta_V \rightarrow \infty$ oscillations are purely temporal. The upper and lower limits to the particle's momentum are $u_{\max} = (\Gamma + u_{+0} + u_{-0})/2$ and $u_{\min} = -(\Gamma - u_{+0} - u_{-0})/2$. The drift velocity (36) reduces to $\bar{u} = (u_{+0} + u_{-0})/2$. For $u_{\pm 0} = 0$, particles oscillate symmetrically between $u_{\min} \approx -u_{\max} \approx \tilde{E}_0^2/4n_-$ and u_{\max} . It is interesting to note that the proportionality $1/\beta_V$ in (37) is similar to that predicted from the single-particle treatment (Rowe 1992b). However, since the single-particle formalism does not include the feedback effect of particles on the wave, it predicts a low drift velocity $\beta_D \approx 1/\beta_V$. Our exact treatment shows that the drift motion can be highly relativistic with $\gamma_D \equiv 1/(1 - \beta_D^2)^{1/2} \approx |\bar{u}| \gg 1$. As a result, the LAEW can drive a relativistic outflow of particles even when the particles are initially at rest. Thus, the oscillating gap can supply relativistic pairs to the pulsar wind.

An implication of such drift motion is that polar cap overheating can be avoided and so, the model satisfies the observational constraint on thermal X-rays from the polar caps. The observed relatively low fluxes of thermal X-rays imply either that the flux of particles that impact on the polar cap is much lower than the GJ flux $\sim |\rho_{GJ}|c$ or that acceleration of returning particles is insignificant. The latter can be ruled out as the returning particles must be subject to the same strong accelerating electric field that accelerates forward moving particles. In the oscillatory model, since particles are dragged forward by the LAEW and escape to infinity, few particles are reflected back to the star; oscillating particles do not impact on the polar cap if the oscillating region is located a distance $> c\tilde{T}/\omega_{GJ} \approx \lambda/\beta_V \sim 0.9$ m for $B = 10^8$ T and $P = 0.1$ s. So, the model can satisfy the observational limit to the thermal X-ray observations from the polar cap. It is worth commenting that by contrast, Ruderman & Sutherland (1975)'s 'vacuum sparks' model, which is intrinsically time dependent, predicts a much larger thermal X-ray flux than the observational limit.

3.4 Currents

The current $j(\chi)$ can be derived using (34). Assuming $\beta_V \gg 1$, we have

$$j_{\parallel} \approx \left(1 - \frac{\beta_{+0}}{\beta_V}\right) \beta_{+} n_{+} - \left(1 - \frac{\beta_{+0}}{\beta_V}\right) \beta_{-} n_{-} + \frac{1}{\beta_V} (\beta_{+}^2 n_{+} - \beta_{-}^2 n_{-}). \quad (38)$$

For half the phase of an oscillation, the electrons and positrons are accelerated in opposite directions, and then these directions reverse, with only a brief phase in which the motion is nonrelativistic. Hence, one has $\beta_{+} \sim -\beta_{-} \sim 1$ for nearly all phases. The final term in Eq (38) is generally small, and on neglecting it, the current is $j_{\parallel} \approx \pm 2n_-$ except for the short phase where it switches sign. Thus, the

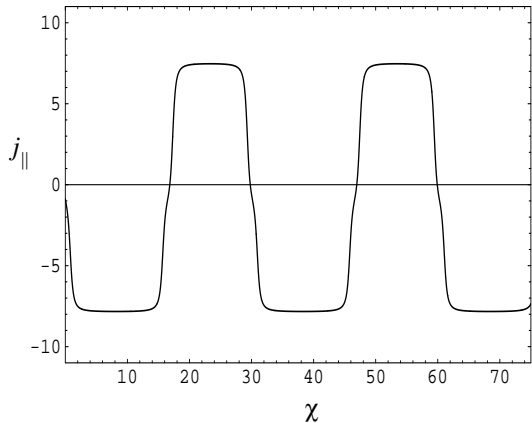


Figure 7. Current j_{\parallel} vs χ . The parameters are as in figure 5. The square wave form can be understood as that in each oscillation particles stay most time in the relativistic regime in which $\beta_{\pm} \sim 1$.

oscillating current has a square wave form with an amplitude $|j_{\max}| \sim 2n_- \gg |j_{0\parallel}|$. A numerical calculation of $j_{\parallel}(\chi)$ is shown in figure 7. Note that as we consider only electrostatic waves, so that the oscillating current induces electric fields only; there is no oscillating magnetic field.

The average current is given by

$$\bar{j}_{\parallel} \approx \bar{\beta}_+ n_+ - \bar{\beta}_- n_- \approx \bar{\beta}(n_+ - n_-), \quad (39)$$

where $\bar{\beta}_{\pm}$ is the mean velocity, i.e., drift velocity. The second approximation is derived for $n_{\pm} \gg 1$ and hence $\bar{\beta}_+ \approx \bar{\beta}_-$. The mean charge density is given by $\bar{\eta} = \eta_{GJ} + (\bar{j}_{\parallel} - j_{0\parallel})/\beta_V$. The system tends to settle into a state where $\bar{\eta} = \eta_{GJ}$ and $\bar{j}_{\parallel} = j_{0\parallel}$.

3.5 Wave dissipation

So far we neglect dissipation in obtaining our solution for LAEW. This is justified if damping (or growth) is weak in the sense that the change in the LAEW in an oscillation period can be treated as a perturbation. Damping occurs through radiative losses, which include curvature radiation, RICS, two-stream instability, and linear acceleration emission (LAE) (Melrose 1978). In the first and second mechanisms, energy losses occur through pair creation. In the third mechanism, plasma instability can arise from counterstreaming of electrons and positrons in oscillations. In the fourth mechanism, particles accelerated in LAEW directly emit electromagnetic radiation, which has close analogy to synchrotron radiation or inverse Compton scattering. It can be shown that damping due to these radiation processes is indeed weak, with the damping time being much longer than the wave period and generally longer than the light-crossing time over the gap. Although in principle one may determine the damping from (2)–(5), averaged over a wave period (Asseo, Kennel & Pella 1977), here in estimating the effect of wave damping, we adopt a different approach in which the wave damping is related to energy losses by a single particle.

To estimate the damping time we consider how the total wave energy density evolves. The total wave energy density can be written as a sum of the electric energy density, $U_E = \varepsilon_0 E^2/2$, and the energy density associated with

particle oscillations, $U_p = m_e c^2 \gamma_{\max}(n_+ + n_-) N_{GJ}$. Using $\gamma_{\max} \approx u_{\max} \approx e^2 E^2 / (m_e^2 c^2 \omega_{GJ})$ (cf. Sec 3.2), one finds $U_p \approx U_E$. Let the average energy loss for a single particle be $\langle \dot{\gamma} \rangle$, where the average is taken over one wave period. The typical damping time scale can be estimated from

$$\tau \approx -\frac{U_E + U_p}{(n_+ + n_-) N_{GJ} \langle \dot{\gamma} \rangle m_e c^2} \approx -\frac{2\gamma_{\max}}{\langle \dot{\gamma} \rangle}. \quad (40)$$

As an example, for curvature radiation, one has $\dot{\gamma}_{\text{curv}} = -(2r_e c / 3R_c^2) \gamma^4$, where $r_e \approx 2.8 \times 10^{-15}$ m is the classical electron radius. Using the average $\langle \gamma^4 \rangle \approx 0.4 \gamma_{\max}^4$ in the limit $\beta_V \gg 1$, one obtains $\langle \dot{\gamma}_{\text{curv}} \rangle \approx -0.4(2r_e c / 3R_c^2) \gamma_{\max}^4$. For $R_c \approx 3 \times 10^5$ m and $\gamma_{\max} = 10^6$, one has $\tau \approx 7.5 R_c^2 / (r_e c \gamma_{\max}^3) \approx 0.8$ s. Thus, the damping time is much longer than the wave period ($2\pi/\omega$) and considerably longer than the light-crossing time over the gap, denoted by τ_g . In general, one has $\tau_g \leq R/c \approx 3 \times 10^{-4}$ s. A similar estimate can be obtained for other three processes and it can be shown that our assumption $\tau \gg 2\pi/\omega$ is valid and that in general $\tau > \tau_g$. For fast pulsars, curvature radiation may become efficient, as a result of a smaller curvature radius, and the damping time may become comparable or even shorter than τ_g , but it is still much longer than the wave period. Similarly, for high magnetic field pulsars ($B > B_c$) with hot polar caps, resonant inverse Compton scattering (Sturmer 1995) (cf. Sec 4.2) can be efficient and can also lead to $\tau \leq \tau_g$.

4 PAIR CREATION

In this section we discuss pair creation occurring in a LAEW. The dominant pair production process is single photon decay in superstrong magnetic fields. We consider two main emission processes that produce pair-producing photons: curvature radiation and resonant inverse Compton scattering (RICS) (Sturmer 1995; Luo 1996). The latter is inverse Compton scattering in cyclotron resonance, involving scattering of thermal photons from the star's surface by relativistic electrons or positrons. Although other processes such as nonresonant inverse Compton scattering may also contribute to pair production, we only focus these processes. How pair creation affects the wave depends on the ratio of the pair production free path, λ_p , and the wavelength, λ . For $\lambda_p/\lambda \gg 1$, a photon travels many wavelengths before it decays into a pair. Pair injection can be treated as nonoscillatory, with the injection rate derived from a sum over the pair production during many oscillations. In the opposite limit $\lambda_p/\lambda \ll 1$, pair creation is locked in oscillations: pairs are injected at particular phase during each oscillation. Here we only discuss the first limit as it is applicable for typical pulsars.

4.1 Curvature radiation

The free path for pair production can be written as $\lambda_p = \Delta s_i + \Delta s_p$, where Δs_i is the characteristic length for emission of a photon at energy $> 2m_e c^2$ and Δs_p is the path length that the photon needs to travel before decay into a pair. For curvature radiation one can show that the former is much shorter than the latter. To estimate Δs_i one writes the production rate, $dn_{\text{ph}}^{(\pm)}/dt$, of forward (+) and

backward (−) propagating curvature photons at the energy ε_c as a ratio of the radiation power, $P_{\text{curv}} \sim -\dot{\gamma}_{\text{curv}}$, to the characteristic energy, ε_c , of curvature photons emitted by a relativistic electron moving along a curved field line with a curvature radius, R_c . Using $dn_{\text{ph}}^{(\pm)}/dt \approx -\dot{\gamma}_{\text{curv}}/\varepsilon_c$, where $\varepsilon_c \approx (3\lambda_c/2R_c)\gamma^3 = 2P_{0.1}^{-1/2}(\gamma/10^6)^3$, and $\lambda_c = \hbar/m_e c \approx 3.86 \times 10^{-13}$ m is the Compton wavelength, one obtains

$$\frac{dn_{\text{ph}}^{(\pm)}}{dt} \approx \frac{\alpha_f c}{R_c} \gamma, \quad (41)$$

where $\alpha_f \approx 1/137$ is the fine constant. Since $dn_{\text{ph}}^{(+)}/dt \approx dn_{\text{ph}}^{(-)}/dt$ for $z \ll R$, the forward and backward components are approximately symmetric. For a dipole magnetic field, the curvature radius is given by $R_c = (4/3)(crP/2\pi)^{1/2} \approx 2.9 \times 10^5 (r/R_0)^{1/2} P_{0.1}^{1/2}$ m. We have

$$\Delta s_i \approx \frac{R_c}{\alpha_f \gamma_{\text{th}}} \approx 13.7 P_{0.1}^{1/2} \left(\frac{10^6}{\gamma_{\text{th}}} \right) \text{ m}. \quad (42)$$

A photon with energy $\varepsilon_\gamma \sim \varepsilon_c > 2$ needs to travel a further distance before being converted to a e^\pm pair. This distance can be estimated as follows. The opacity of a photon in a strong magnetic field is a function of $\psi = 0.5\varepsilon_B \varepsilon_\gamma \sin \theta_{\gamma B}$, where $\theta_{\gamma B}$ is the propagation angle of the photon and $\varepsilon_B = B/B_c$ (Erber 1966). Generally, pair creation requires $\psi \sim 1/15$. A pair is produced when the opacity reaches unity. Using $\theta_{\gamma B} \sim \Delta s_p/R_c$, one has $\Delta s_p = 2\psi R_c/\varepsilon_B \varepsilon_c$ to produce one pair. Since the maximum γ is limited by radiation-reaction, denoted by γ_R , one may obtain a lower limit to the free path,

$$\lambda_p = \frac{R_c}{\varepsilon_{c,R}} \left[\frac{\varepsilon_{c,R}}{\alpha_f} \left(\frac{3\lambda_c}{2R_c} \right)^{1/3} + \frac{2\psi}{\varepsilon_B} \right], \quad (43)$$

where $\varepsilon_{c,R} = (3\lambda_c/2R_c)\gamma_R^3$. The right-hand side is ~ 500 m for $R_c = 3 \times 10^5$ m, $\psi = 0.01$, $\varepsilon_B = 0.1$, $\varepsilon_\gamma = \varepsilon_{c,R} = 10^2$. Using the parameters in (11) one has $\lambda < \lambda_p$ for $\beta_V < 5 \times 10^2$.

4.2 Resonant inverse Compton scattering

Similarly, one may estimate λ_p for RICS. For thermal photons at energy $\Theta < 1/\gamma$, one can ignore the Klein-Nishina effect; the production rate of the scattered photon at energy $\varepsilon_s \sim \varepsilon_B \gamma$ is (Sturmer 1995; Luo 1996)

$$\frac{dn_{\text{ph}}^{(\pm)}}{dt} \approx \frac{9x^{(\pm)}\Theta\varepsilon_B c\sigma_{\text{eff}}}{8\pi^2\gamma^2 \lambda_c^3}, \quad (44)$$

where $\Theta = 1.7 \times 10^{-4}(T_s/10^6 \text{ K})$ is the normalized temperature T_s of the polar cap, $\sigma_{\text{eff}} \approx 3\pi\sigma_T/4\alpha_f$ is the effective cross section of RICS, and $x^{(\pm)} = -\ln[1 - \exp(-\varepsilon_B/\Theta\gamma(1 \mp \beta \cos \theta_m))]$ with θ_m the maximum propagation angle of the incoming photon (Dermer 1990). Since $x^{(-)} > x^{(+)}$, pair production by particles moving toward the star is more efficient than particles moving away from the star (Harding & Muslimov 1998). For both cases, the rate increases with decreasing γ . However, the process becomes less efficient at low energy as the cyclotron resonance condition becomes difficult to satisfy ($x^{(\pm)}$ decreases exponentially when γ is too low for the condition to be satisfied). This leads to an estimate of Δs_i :

$$\Delta s_i \approx 10^4 \varepsilon^{1/3} \left(\frac{T_s}{10^6 \text{ K}} \right)^{-2/3} \left(\frac{x_\pm}{0.5} \right)^{2/3} B_8^{-4/3} P_{0.1}^{1/6} \text{ m}. \quad (45)$$

We write γ as a fraction $\varepsilon \ll 1$ of the maximum potential drop across the polar cap. Since $\Theta < 1/\gamma$, one has

$$\Delta s_p = \frac{2\psi R_c}{\gamma\varepsilon_B} > 2\psi R_c \frac{\Theta}{\varepsilon_B}. \quad (46)$$

For $\Theta = 1.7 \times 10^{-4}$ and $\varepsilon_B = 0.1$, one has $\Delta s_p \approx 23$ m. One concludes that for a moderate $\beta_V > 1$, $\lambda_p \gg \lambda$ applies to RICS. For $\gamma > 1/\Theta$, the scattering is in the Klein-Nishina regime, which is not discussed here.

4.3 Pair injection

Since for $\lambda_p \gg \lambda$, one may regard $dn_{\text{ph}}^{(\pm)}/dt$ as a constant, where γ is replaced by its average (over the period). One may write the source term in (7) as

$$Q = \frac{1}{2}(\alpha_+ N_+ + \alpha_- N_-), \quad (47)$$

where $\alpha_\pm = \langle dn_{\text{ph}}^{(+)}/dt \rangle + \langle dn_{\text{ph}}^{(-)}/dt \rangle$ is a constant. It should be noted that inclusion of higher generations of pairs is necessary in conventional treatments of pair creation in a pair formation front, especially for curvature radiation. Inclusion of higher generations would effectively increase α_\pm in (45). However, the assumption that the free path for pair production is much longer than the wavelength remains valid.

Assuming $\beta_V \gg 1$, integration of (7) results in an exponential growth

$$N_\pm \approx n_\pm \exp\left(\frac{\bar{\alpha}_+ + \bar{\alpha}_-}{2\beta_V} \chi\right), \quad (48)$$

where $\bar{\alpha}_\pm = \alpha_\pm/\omega_{GJ}$. One can show that for $\chi \sim \beta_V \omega_{GJ} t$ as $\beta_V \gg 1$, Eq (48) reduces to $N_\pm \propto \exp[-(\alpha_+ + \alpha_-)t/2]$, which reproduces the numerical result in Levinson et al. (2005).

We envisage pair creation as being only a minor perturbation except when the large-amplitude oscillation is being set up, as described in the purely temporal case by Levinson et al. (2005). Here one may derive the condition under which the effect of the source function in the equation of motion (8) can be ignored. This effect can be characterized by a parameter $\delta_\pm \equiv \bar{Q}/2\beta_V \bar{N}_\pm$, where we assume $\beta_V \gg 1$. The pair production has only a minor effect if $\delta_\pm \ll 1$. Using (47) and (48), this condition can be written in the form $\delta_\pm = (\alpha_+ n_+ + \alpha_- n_-)/(4\beta_V \omega_{GJ} n_\pm) \ll 1$. As an example, for curvature radiation one has $\delta_\pm \sim 2^{m_g-1} \alpha_f c \gamma / 2R_c \beta_V \omega_{GJ} \ll 1$, where one assumes there are m_g generations of pairs.

5 LOW-DENSITY LIMIT

The low-density regime is applicable if there are initially insufficient charges to provide the GJ charge density. One can show that in this limit both monotonic and oscillatory solutions exist, with the former corresponding to rapid acceleration of charged particles from the surface.

5.1 Monotonic acceleration

A relevant example of a low density corresponds to a space-charge-limited flow (SCLF) from the surface, which has

so far been discussed only in the context of the steady state (Arons & Scharlemann 1979; Mestel & Shibata 1994; Harding & Muslimov 1998). The case of a vacuum-like field is applicable for pulsars with $\boldsymbol{\Omega} \cdot \mathbf{B} < 0$ when ions are tightly bound to the surface (Medin & Lai 2007). This case was considered in Levinson et al. (2005) and is not discussed here. We consider an outflow of electrons from the polar cap with $\boldsymbol{\Omega} \cdot \mathbf{B} > 0$. The initial electric field at the surface is assumed to be small. Assuming $n_+ = 0$, one obtains

$$\Phi = \tilde{E}_0^2 + 2 \left[(\gamma - \gamma_0) \eta_{GJ} - (u - u_0) j_{0\parallel} \right], \quad (49)$$

where (14) is used. A solution for $\Phi > 0$ is $j_{0\parallel} < \eta_{GJ}$ for $u > u_0 \geq 0$. As shown in figure 8, u only has a lower bound, corresponding to the positive part of the solid and dashed lines, and in these cases electrons can be accelerated monotonically outward. When $j_{0\parallel} > \eta_{GJ}$ (dotted line), u has both upper and lower bounds and the solution must be oscillatory with the upper bound being well below the pair production threshold. Such low amplitude oscillatory solution was also discussed recently (Beloborodov 2007). It should be pointed out here that the effect of the conducting wall is not considered but can become dominant in determining the acceleration (see further comments in Sec 5.2). For $\beta_V \gg 1$ one has $d\xi \approx -\beta_V du$ in (22), which gives rise to a monotonic solution for the electric field:

$$\tilde{E}_{\parallel} \approx \tilde{E}_0 - \frac{\delta\eta}{\beta_V} \chi, \quad (50)$$

with $\delta\eta = \eta_{GJ} - j_{0\parallel} > 0$ and $\tilde{E}_0 < 0$. The electron's momentum increases according to

$$u_- \approx u_{-0} + \frac{|\tilde{E}_0|}{\beta_V} \chi + \frac{\delta\eta}{2\beta_V^2} \chi^2. \quad (51)$$

A special case is an initial phase $\chi = 0$ chosen corresponding to $t = 0$ and $z = 0$, i.e., at the surface where one has $\tilde{E}_0 \approx 0$. We envisage that \tilde{E}_{\parallel} grows to reach the value at which pair production occurs and the oscillatory phase takes over with \tilde{E}_0 in Sec 3 replaced by the threshold \tilde{E}_{\parallel} . The acceleration discussed here is different from the usual SCLF models; the electric field is predominantly inductive.

In the temporal case, an electric field increases linearly with time and thus, the 4-velocity of the particles varies quadratically with time: $u_- \propto \delta\eta \tilde{t}^2/2$ with $\tilde{t} = \omega_{GJ} t$. The time for an electron to be accelerated to the pair production threshold γ_{th} is

$$t = \frac{2}{\omega_{GJ}} \left(\frac{\gamma_{th}}{|\delta\eta|} \right)^{1/2}. \quad (52)$$

The time (52) should be limited by the travel time of a particle across the acceleration region. Assuming the region to have a size of ΔL , the limit gives rise to a condition $t < \Delta L/c$ for a pair cascade to occur.

In general, the relative importance of acceleration due to inductive and non-inductive (potential) electric fields can be determined from $(u_-)_{\text{inductive}} / (u_-)_{\text{static}} \sim \beta_V^2$. For $\beta_V^2 \gg 1$, inductive acceleration is dominant. The acceleration can be regarded as purely electrostatic only in the special case $\beta_V \rightarrow 0$, which is discussed in 5.2.

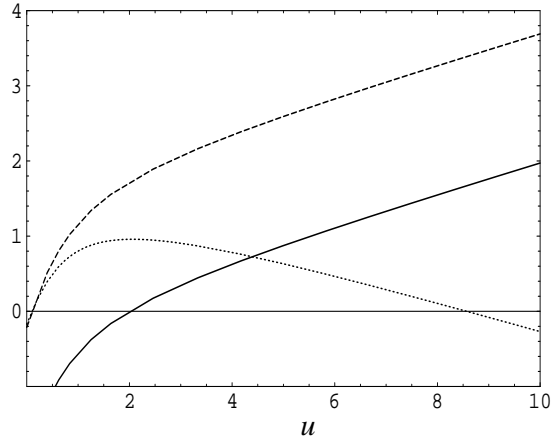


Figure 8. Plot of Φ as a function of u in the low-density limit for $(\eta_{GJ}, j_{0\parallel}) = (-1, -1.1)$ with $u_{-0} = 2$ (solid), $(\eta_{GJ}, j_{0\parallel}) = (-1, -1.1)$ with $u_{-0} = 0.1$ (dashed) and $(\eta_{GJ}, j_{0\parallel}) = (-1, -0.9)$ with $u_{-0} = 0.1$ (dot). The third case only permits an oscillatory solution with u being limited by $\leq u_{\text{max}} \approx 8.5$. The initial electric field is assumed to be $\tilde{E}_0 = 0$.

5.2 Comparison with the steady-state models

The steady state can be regarded as a limit $\beta_V \rightarrow 0$ in which the parallel electric field is purely static. For $\beta_V \rightarrow 0$ the phase depends on spatial coordinates only and can be written as $\chi = -\omega_{GJ} z/c \equiv -\tilde{z}$. Substituting (49) into (22) and using $d\xi \approx d\gamma$, one obtains

$$\tilde{E}_{\parallel} = \tilde{E}_0 - \delta\eta \tilde{z}, \quad (53)$$

where $\tilde{E}_0 < 0$. The monotonic solution (53) can be regarded as an oscillatory solution in the long period limit $\tilde{T} \rightarrow \infty$. From the current-charge invariant (13) one has $\eta(0) - \eta_{GJ} = -(\beta_{-0} n_- + j_{0\parallel})/\beta_V$. Since $\eta(0) - \eta_{GJ}$ must remain finite, the limit $\beta_V \rightarrow 0$ implies that the initial current is $j_{\parallel}(0) \approx -\beta_{-0} n_-$, which matches the constant current $j_{\parallel}(0) = j_{0\parallel}$. The electron's momentum is derived as

$$u_- = u_{-0} + |\tilde{E}_0| \tilde{z} + \frac{1}{2} \delta\eta \tilde{z}^2. \quad (54)$$

As for (50), for electrons to be accelerated outward one must have $\delta\eta > 0$. That the same condition ($\delta\eta > 0$) is required in both cases is hardly surprising. In (50), one has $d\xi \sim -\beta_V du < 0$ and $\chi > 0$, while in (50) one has $d\xi \sim du > 0$ but $\chi < 0$. If $\tilde{E}_0 \sim 0$, the electron's momentum increases with \tilde{z} quadratically, $u_- \sim \delta\eta \tilde{z}^2/2$.

In the conventional SCLF models (Arons & Scharlemann 1979; Harding & Muslimov 1998), $E_{\parallel} < 0$ is obtained with $\delta\eta < 0$, by imposing an upper boundary, usually located at the PFF, where $E_{\parallel} = 0$, and a conducting surface of the side wall of the open field line region; in these models $j_{0\parallel}$ is then determined locally by these boundary conditions. The basic assumption in the SCLF models is the nonconstancy of $\delta\eta$ along flow. This means that if one sets $\delta\eta = 0$ initially, a nonzero $\delta\eta \neq 0$ develops along the flow inducing a parallel electric field. Two effects that lead to $\delta\eta < 0$ have been considered in the literature, including field line curvature, corresponding to the field lines curving toward the rotation axis, and frame dragging (Muslimov & Tsygan 1992). The latter dominates near the star; the effective angular velocity, so is the GJ density, is reduced by a factor $(1 - k_g(R/r)^3) < 1$

as compared to that observed in a flat space at infinity, where $k_g = 2GI/(c^2 R^3) \approx 0.15I_{38}$, $z < R = 10^4$ m, and $I_{38} = I/(10^{38} \text{ kg m}^2)$ is the moment of inertia of the star (Muslimov & Tsygan 1992). If one assumes $\delta\eta = 0$ initially at the surface, one has $\delta\eta = 3k_g\eta_{GJ}z/R < 0$ for $\eta_{GJ} < 0$.

Eq (53) and (54) are similar to the result derived by Shibata (1997) based on a generic SCLF model in which no specific local boundary condition is imposed. When $j_{0\parallel}$ is treated as a free parameter, for initially $\delta\eta = 0$, $\delta\eta > 0$ is required to produce $E_{\parallel} < 0$. This can occur only on the curving-away (from the rotation axis) field lines along which $|\boldsymbol{\Omega} \cdot \mathbf{B}|$ decreases (Shibata 1997; Mestel 1999). A major problem with this scenario in the context of the steady-state limit is that the growth in $|E_{\parallel}|$ is unstoppable (Shibata 1997; Mestel 1999). However, such run-away growth does not occur in our oscillatory model because pair creation ultimately leads the system to switch to an oscillatory phase, as discussed in Sec. 3. For $\delta\eta < 0$, Eq (54) implies an oscillatory (in space) solution similar to that found previously (Mestel & Shibata 1994; Shibata 1997). When the acceleration region extends to $> R(R/R_{LC})^{1/2}$, the effect of the conducting side wall, at which $E_{\parallel} = 0$, becomes important. When such effect is included acceleration of outflowing electrons is possible at $> R(R/R_{LC})^{1/2}$ even when $\delta\eta < 0$ (provided that an electric field arising from such effect dominates over that from $\delta\eta < 0$) (Shibata 1997).

6 CONCLUSIONS AND DISCUSSION

We present an oscillatory polar gap model, in which the system initially undergoes a low-density phase, involving rapid acceleration of particles to ultra high energy, initiating a pair cascade. The system evolves to an oscillatory phase. The oscillations are treated as a superluminal, large amplitude electrostatic wave that propagates along the magnetic field. The charge continuity equation implies a current-charge invariant ($j_{\parallel} - \beta_V\eta = \text{const}$) that is independent of pair creation. As a result, the phase velocity β_V is no longer a free parameter and can be written in terms of the initial velocity and density of the plasma. It is shown that only the superluminal case $\beta_V > 1$ is relevant here. An analytical formalism for LAEWs is derived in the high-density regime in which the pair density is higher than the GJ density. We ignore wave damping in our analytical solution. Neglecting damping is justified as the typical damping time due to energy losses through radiation is much longer than the wave period. In most cases, the damping time is also longer than the light-crossing time over the gap.

The model predicts an outflow of relativistic pairs due to particles being dragged along in LAEW. Such feature is needed to avoid overheating of the polar cap. Outflowing pairs would contribute to the pulsar wind. Pairs oscillate with a net drift velocity directed along the magnetic field, producing a current that oscillates about the global constant current j_0 . The amplitude of the oscillating current is larger than the global current by a large factor that is of order of magnitude the ratio of the pair density to the GJ density. The wave form of an inductive electric field is characterized by a triangular shape, which can be understood as the current being nearly constant except for a brief period during which it switches sign. The basic features of the oscillations

are not sensitive to the initial conditions including the electron's or positron's initial velocity.

There are two possibilities for particle acceleration in the initial phase that leads to oscillations: (1) a vacuum-like initial electric field, which may be applicable for the polar cap where charges are tightly bound to the surface, and (2) SCLF, in which there is an ample supply of charges. The first case was discussed in Levinson et al. (2005). Here we consider specifically the SCLF case where an initial electric field appears as a result of an imbalance between the charge density and the GJ density with the latter mimicking the positive background charges. Electrons are accelerated monotonically in the electric field that increases linearly with the phase χ . Since χ comprises both temporal and spatial variables, such particle acceleration arises from a mixture of inductive and non-inductive effects. An interesting limit is $V \rightarrow \infty$, in which the electric field becomes purely inductive. Qualitatively, the usual steady-state theory can be reproduced in the limit of a zero phase speed. In this limit, the system is time independent and the acceleration occurs at a specific spatial location. By contrast, acceleration due to an inductive field can occur everywhere in the region concerned.

An implication of the oscillatory model is the prediction of plasma instability arising from counterstreaming of electrons and positrons; in each oscillation electrons and positrons are accelerated in opposite direction and such counterstreaming provides an ideal condition for two-stream instability which may be directly relevant for pulsar radio emission (Verdon & Melrose 2007). Although various forms of streaming instability have been discussed in connection with the radio emission in conventional models, the growth rate is generally too low to be effective, requiring some separate assumption to enhance it. In the oscillatory model, the relative streaming of electrons and positrons allows the maximum possible growth rate for the two-stream instability, at phases where the counterstreaming is nonrelativistic or mildly relativistic. Apart from the two-stream instability, LAE may also operate in conversion of LAEW to electromagnetic radiation.

In an oscillatory pulsar magnetosphere, cyclotron resonance can have a significant effect on the propagation of the coherent radio emission. In the conventional polar cap models, for a wave propagating at an angle θ to the magnetic field, the cyclotron resonance occurs preferentially in the large-angle regime $\theta \gg 1/\gamma$ at a frequency $\omega = \Omega_e/\gamma\theta^2$, located at a radius, which is generally in the outer magnetosphere, $r_c \sim (\Omega_{e0}/\gamma\theta^2\omega)^{1/3}$, where Ω_{e0} is the cyclotron frequency at the surface (Luo & Melrose 2001). In the oscillatory pulsar magnetosphere, the cyclotron resonance can occur at $\omega = \Omega_e/2\gamma$ for particles moving toward the star. The cyclotron radius r_c varies with oscillating γ , with the smallest radius being $(r_c)_{\min} \approx (\Omega_{e0}/2\gamma_{\max}\omega)^{1/3}$; This radius is smaller than in the usual polar cap models by a factor $(\theta^2/2)^{1/3} \approx 0.17$ for $\theta = 0.1$.

There are some limitations of our model, notably the one-dimensional assumption that may not be realistic for an acceleration region extended beyond $> R(R/R_{LC})^{1/2}$. The effect of the side wall of the open field line region needs to be included in the calculation. Such region can be modeled as a wave guide and propagation of LAEWs in such wave guide will be discussed elsewhere. Nonetheless, from

this one-dimensional, analytical model we are able to derive some fundamental features of LAEWs that should remain valid qualitatively for a more general, three-dimensional case as well. The fluid treatment adopted here may not be accurate for pulsar plasma as numerical simulations showed that pairs from a cascade generally have a broad distribution (Arendt & Eilek 2002) and inclusion of a particle distribution requires a kinetic formalism which is beyond the scope of this paper.

ACKNOWLEDGEMENTS

We thank Mike Wheatland for helpful comments.

REFERENCES

- Akhiezer, A. I., Akhiezer, I. A., Polovin, R. V., Sitenko, A. G., Stepanov, K. N., 1975, *Plasma Electrodynamics Vol. 2*, Pergamon Press
- Arendt, P. N., Eilek, J., 2002, *ApJ*, 581, 451
- Arons, J., Scharlemann, E., 1979, *ApJ*, 231, 854
- Arons, J., 1983, *ApJ*, 266, 215
- Asseo, E., Kennel, C. F., Pella, R., 1977, *A&A*, 65, 401
- Beloborodov, A. M., 2007, astro-ph0710.0920
- Blaskiewicz, M., Cordes, J., Wasserman, I., 1991, *ApJ*, 370, 643
- Cheng, A., Ruderman, M., 1976, *ApJ*, 203, 209
- Cheng, K. S., Ho, C., Ruderman, M., 1986, *ApJ*, 300, 500
- Dermer, C. D., 1990, *ApJ*, 360, 197
- Erber, T., 1966, *Rev. Mod. Phys.*, 38, 626
- Everett, J. E., Weisberg, J. M., 2001, *ApJ*, 553, 341
- Fawley, W. M., Arons, J., Scharlemann, E. T., 1977, *ApJ*, 217, 227
- Harding, A., Muslimov, A., 1998, *ApJ*, 508, 328
- Harding, A., Muslimov, A., 2005, *Ap&SS*, 297, 63
- Hirovani, K., 2006, *ApJ*, 652, 1475
- Levinson, A., Melrose, D. B., Judge, A., Luo, Q., 2005, *ApJ*, 631, 456
- Luo, Q., 1996, *ApJ*, 468, 338
- Luo, Q., Melrose, D. B., 2001, *MNRAS*, 325, 187
- Medin Z., Lai D., 2007, *Advances in Space Research* (in press)
- Melrose, D. B., 1978, *ApJ*, 225, 557
- Melrose, D., Levinson, A., Judge, A., Luo, Q., 2005, *AIP Proceedings*
- Mestel, L., 1999, *Stellar Magnetism*, Clarendon Press: Oxford
- Mestel, L., Shibata, S., 1994, *MNRAS*, 271, 621
- Michel, F. C., 2004, *Adv. Space Res.* 33, 542
- Michel, F. C., 1975, *ApJ*, 197, 193
- Muslimov, A. G., Tsygan, A., 1992, *MNRAS*, 255, 61
- Rowe, E. T., 1992, *Aust. J. Phys.* 45, 1
- Rowe, E. T., 1992, *Aust. J. Phys.* 45, 21
- Romani, R., 1996, *ApJ*, 470, 469
- Ruderman, M. A., & Sutherland, P. G. 1975, *ApJ*, 196, 51
- Scharlemann, E. T., Wagoner, R. V., 1973, *ApJ*, 182, 951
- Shibata, S., 1991, *ApJ*, 378, 239
- Shibata, S., 1997, *MNRAS*, 287, 262
- Sturmer, S. J., 1995, *ApJ*, 446, 292
- Sturrock, P. A. 1971, *ApJ*, 164, 529
- Thompson, D. J., 2001, in *High Energy Gamma-Ray Astronomy*, AIP Proceedings, vol 558, p. 103
- Timokhin, A. N., 2006, *MNRAS*, 368, 1055
- Verdon, M., Melrose, D. B., 2008, in *40 Years of Pulsars—Millisecond Pulsars, Magnetars, and More*, eds C. G. Bassa, Z. Wang, V. M. Kaspi, AIP Conf. Proc. Vol 983, p. 133

APPENDIX A: DERIVATION IN THE TEMPORAL GAUGE

In this appendix, we outline an alternative derivation of the wave equation in the temporal gauge. Electric and magnetic fields can be expressed in terms of a vector potential

$$\mathbf{E} = -\frac{\partial \mathbf{A}}{\partial t} \quad \mathbf{B} = \nabla \times \mathbf{A}. \quad (\text{A1})$$

From (5) we have

$$\nabla(\nabla \cdot \mathbf{A}) - \nabla^2 \mathbf{A} + \frac{1}{c^2} \frac{\partial^2 \mathbf{A}}{\partial t^2} = \mu_0(\mathbf{J} - \mathbf{J}_R). \quad (\text{A2})$$

Assuming that all the relevant quantities are functions of χ , the parallel (to $\boldsymbol{\kappa}$) component of (A2) takes the form

$$\frac{d^2 A_{\parallel}}{d\chi^2} = \frac{\mu_0}{\beta_V^2} (J_{\parallel} - J_{0\parallel} - J_{R\parallel}), \quad (\text{A3})$$

with $A_{\parallel} = \boldsymbol{\kappa} \cdot \mathbf{A}$ and

$$\begin{aligned} J_{0\parallel} &= \nabla_{\parallel}(\nabla \cdot \mathbf{A}) - \nabla^2 A_{\parallel} \\ &= \nabla_{\parallel}(\nabla_{\perp} \cdot \mathbf{A}_{\perp}) - \nabla_{\perp}^2 A_{\parallel}. \end{aligned} \quad (\text{A4})$$

The equation of motion (2) can be written into a similar form to (17):

$$(\beta_V - \beta_{s\parallel}) \frac{du_{s\parallel}}{d\chi} = -\frac{se\beta_V}{m_e c} \frac{dA_{\parallel}}{d\chi} + \frac{1}{c} \left(\frac{q_{s\parallel}}{m_e c^2} - \frac{Q}{2N_s} u_{s\parallel} \right), \quad (\text{A5})$$

which can be integrated to yield

$$\begin{aligned} \frac{1 - \beta_V \beta_s}{(1 - \beta_s^2)^{1/2}} - 1 &= \frac{se\beta_V}{m_e c} (A_{\parallel} - A_{0\parallel}) \\ &\quad - \frac{1}{c} \int_0^{\chi} \left(\frac{q_s}{m_e c^2} - \frac{Q}{2N_s} u_s \right) d\chi', \end{aligned} \quad (\text{A6})$$

where $A_{0\parallel} \equiv A_{\parallel}(\chi = 0)$ and $s = \pm$ corresponds to electrons (+) and positrons (-). Assuming $\tilde{A} = (e/m_e c)(A_{\parallel} - A_{0\parallel})$, for the electron component $\beta = \beta_-$, one obtains

$$\begin{aligned} \frac{1}{2} \beta_V^2 \left(\frac{d\tilde{A}}{d\chi} \right)^2 &= \frac{\omega_p^2}{c^2} \left[f - \frac{1}{(1 - \beta^2)^{1/2}} \right. \\ &\quad \left. \times \left(n_- + g\eta_+ - (1 - \beta_V \beta) \frac{j_{0\parallel}}{\beta_V} \right) \right], \end{aligned} \quad (\text{A7})$$

where f is an integration constant. Clearly, a physical solution requires the RHS to be non-negative; this condition can be satisfied only if $\beta_{min} \leq \beta \leq \beta_{max}$, where β_{min} and β_{max} are the minimum and the maximum velocities at which the RHS is zero. The electric field can be found from

$$\tilde{E}_{\parallel} = -\beta_V \frac{d\tilde{A}}{d\tilde{\chi}}. \quad (\text{A8})$$

APPENDIX B: ELECTRON GAS

Here we reproduce the known result for a LAEW in an electron gas, by retaining the electron component only. Specifically, we set $\beta_0 \equiv \beta_{-0} = 0$ and $\eta_+ = \eta_0 = \eta_{GJ} = 0$. The maximum velocity can be expressed in terms of \tilde{E}_0 :

$$\frac{1}{(1 - \beta_m^2)^{1/2}} \equiv \frac{1}{2} \tilde{E}_0^2 + 1. \quad (\text{B1})$$

Eq (22) and (23) reproduce an analytical form similar to that given by Akhiezer et al. (1975):

$$- \int \left[\frac{1}{(1 - \beta_m^2)^{1/2}} - \frac{1}{(1 - \beta^2)^{1/2}} \right]^{-1/2} d\xi = 2^{1/2} \frac{\omega_p}{c} \chi, \quad (\text{B2})$$

$$E_{\parallel} = \pm 2^{1/2} \frac{m_e c}{e} \omega_p \left[\frac{1}{(1 - \beta_m^2)^{1/2}} - \frac{1}{(1 - \beta^2)^{1/2}} \right]^{1/2}. \quad (\text{B3})$$

Consider the relativistic limit $\gamma_m \equiv 1/(1 - \beta_m^2)^{1/2} \gg 1$; Using $\beta \approx \pm(1 - \gamma^{-2}/2)$, one finds

$$\begin{aligned} &2 \left[1 \pm \beta_V \left(1 + \frac{1}{\gamma_m} \right) \right] (\gamma_m - 1)^{1/2} \\ &+ \left[2 \mp \beta_V \left(1 + \frac{1}{2\gamma\gamma_m} \right) \right] (\gamma_m - \gamma)^{1/2} \\ &\pm \frac{\beta_V}{2\gamma_m^{3/2}} \left[\operatorname{arctanh} \left(1 - \frac{1}{\gamma_m} \right) - \operatorname{arctanh} \left(1 - \frac{\gamma}{\gamma_m} \right) \right] \\ &= \sqrt{2} \left(\frac{\omega_p}{c} \right) \chi. \end{aligned} \quad (\text{B4})$$

Since β is a periodic function of χ , we can define a period T by

$$\begin{aligned} &2 \int_{-\beta_m}^{\beta_m} d\beta \frac{\beta_V - \beta}{(1 - \beta^2)^{3/2}} \left[\frac{1}{(1 - \beta_m^2)^{1/2}} - \frac{1}{(1 - \beta^2)^{1/2}} \right]^{-1/2} \\ &= \sqrt{2} \omega_p \beta_V T. \end{aligned} \quad (\text{B5})$$

The RHS can be written into the form in the $\gamma_m \gg 1$ limit:

$$4 \int_1^{\gamma_m} \frac{\beta d\gamma}{(\gamma_m - \gamma)^{1/2}} \approx 8\gamma_m^{1/2}. \quad (\text{B6})$$

If we define a frequency $\omega = 2\pi/T$, (B5) leads to

$$\omega = \frac{\sqrt{2}\pi\omega_p}{4\gamma_m^{1/2}}, \quad (\text{B7})$$

which is similar to (33).